Nonlinear enhancement of locking range of mutually injection-locked oscillators for resonant sensing applications

Jérôme Juillard, Ali Mostafa, Pietro Maris Ferreira

AUTHOR VERSION

Nonlinear enhancement of locking range of mutually injection-locked oscillators for resonant sensing applications

Jérôme Juillard, Ali Mostafa, Pietro Maris Ferreira
Mixed-Signals Circuits and Systems (MiSCaS)
GEEPS, UMR8507, CNRS, CentraleSupélec, UPSud, UPMC
Gif-sur-Yvette, France
jerome.juillard@centralesupelec.fr

***Abstract*— Sensor architectures based on coupled resonators are receiving increased interest from the resonant sensing community. Certain output metrics of such sensors have an increased sensitivity to the measurand, compared to conventional resonant sensors with frequency-modulated outputs. In the present paper, we investigate the properties of a differential architecture based on mutually injection-locked oscillators beyond the linear theoretical framework, by driving the resonators higher than the critical Duffing amplitude. Our results show that a trade-off must be made between sensitivity and measurement (locking) range. Experimental results obtained with our MILO architecture and the amplitude ratio output metric are also reported for the first time.**

Keywords—resonant sensors; coupled resonators; MEMS

I. INTRODUCTION

Recent years have seen the development of several sensor architectures based on coupled MEMS resonators, such as open-loop or closed-loop sensors based on mode-localization [1-4] or on mutually-injection locked oscillators (MILOs) [5-6]. Such sensors usually have output metrics whose sensitivity to the measurand is much greater than those of conventional resonant sensors with frequency-modulated outputs, although this does not necessarily entail a gain in sensor resolution, as was recently shown [7].

MILOs consist in two resonators with nominally identical resonance frequencies and quality factors, placed in a nonlinear feedback loop (Fig. 1) designed so that the resonators oscillate synchronously, typically in quadrature. When a stiffness mismatch ε is induced between the resonators (e.g. electrostatically), the resonance frequencies of the resonators are no longer identical. The nonlinear mixer then ensures that the system remains in a phase-locked state, but with a phase difference which deviates from 90°. The deviation of the phase-difference from its nominal value provides a high-sensitivity measurement of the stiffness mismatch between the resonators, and hence of the quantity of interest. In the particular case considered in this paper, the nonlinear mixer is designed to have maximal phase difference sensitivity to stiffness mismatch, as well as minimal fluctuations of the phase difference [7]. The mixer consists of two comparators, which ensure that the Barkhausen gain criterion is met in both loops, and of a digital coupling stage. Under the hypothesis that both resonators operate in the linear regime, one may show that the phase difference is an "optimal" output metric for this architecture, with maximal sensivity to the measurand and minimal sensitivity to thermomechanical fluctuations [5].

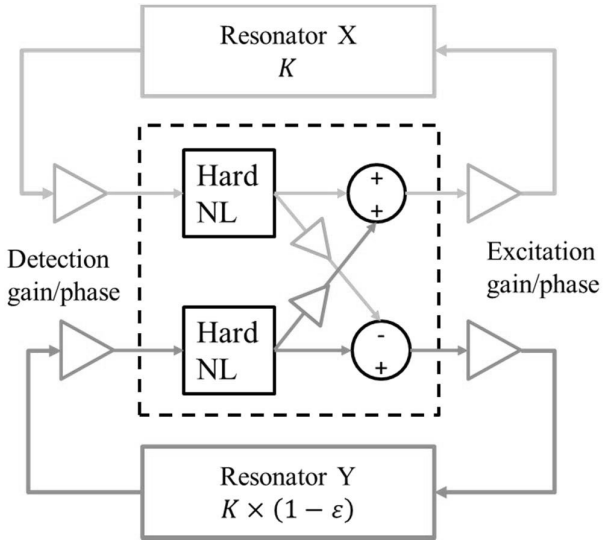

Fig. 1. High-level schematic of a MILO consisting of two resonators with a relative stiffness mismatch ε, a nonlinear mixer and gain/phase adaptation stages.

A key issue in MILOs is the measurement range, i.e. the range of values of ε for which the resonators remain synchronized. In the linear operation regime, this measurement range is inversely proportional to the quality factors of the resonators. Several recent studies [8-9] have pointed out the possibility of extending the synchronization domain of oscillators by operating them in the nonlinear regime. With the present paper and its companion [10], our aim is to investigate, theoretically and experimentally, some of the trade-offs that are entailed by nonlinearly-operated MILOs.

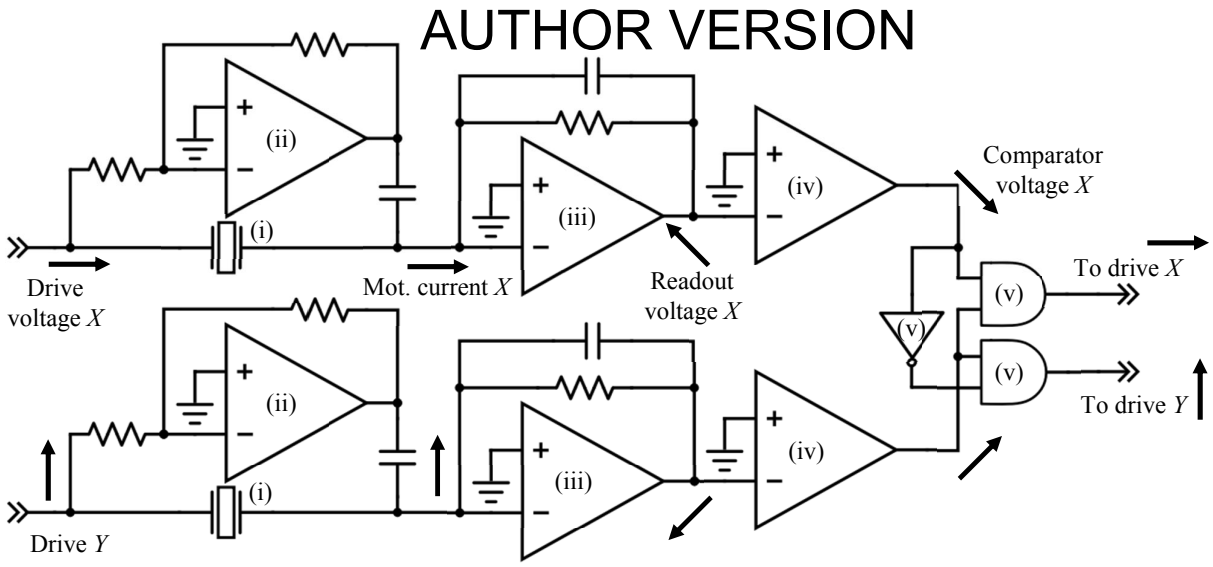

Fig. 2. Schematic of the studied MILO, consisting of resonators (i), feedthrough compensation stages (ii), readout stages (iii), comparators (iv) and logic gates (v). The resistive bridges used for setting drive voltage values have been omitted.The black arrows correspond to the phasor representation of the indicated electrical quantities.

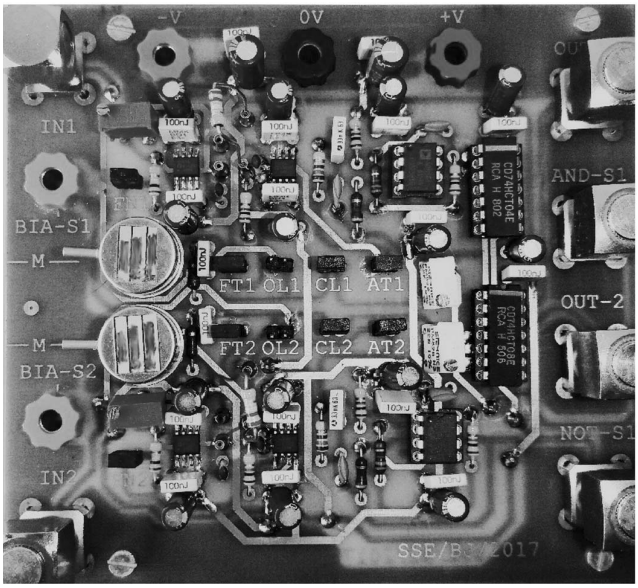

Fig. 3. PCB implementation of the MILO with discrete components.

Section II of this paper is dedicated to a description of our experimental setup. A simple model of the architecture is presented in section III. In section IV, we compare the experimental results to the ones derived from the model. In particular, we report for the first time measurements performed on MILOs with the amplitude ratio output metric. Section V is dedicated to concluding remarks.

EXPERIMENTAL SETUP

A schematic of the experimental setup is shown in Fig. 2, and a photograph of the corresponding printed circuit board (PCB) is shown in Fig. 3. The key elements here are (i) the resonators: these are high-Q (>10^4) capacitively-transduced resonant pressure sensors, with matched resonance frequencies around 70kHz, described at length in [11], (ii) an active feedthrough-cancellation stage, which effectively eliminates direct capacitive coupling between the input port and output port of the resonator, (iii) the analog readout stage, whose feedback impedance (half-resistive, half-capacitive) sets the phase in the loop and determines which oscillation mode is selected, and a digital mixer consisting of (iv) two comparators and (v) three logic gates. If feedthrough is correctly compensated, the current at the input of the readout stage is purely motional, and is thus in phase with the velocity of the resonator. The circuit is designed so that the voltage at the output of the comparator stage has a $-\pi/4$ phase-lag with respect to the motional current, or a $\pi/4$ phase-lead with respect to the mechanical motion. In the absence of mismatch between the resonators, this results in resonator Y oscillating with a $\pi/2$ phase-lead over resonator X, as illustrated in Fig. 2. Moreover, each resonator is then optimally driven at resonance, its drive voltage being in phase with its motional current, so that the influence of additive perturbations on frequency and phase difference stability is minimized, as shown in [5]. Note that the exact amount of delay introduced by each comparator is dependent on the relative amplitude of its input signal to the comparator hysteresis (a few mV).

The resonators can be finely tuned by adjusting their bias voltages. The (mechanical) oscillation amplitude can be adjusted independently by changing the ratio of the potentiometer bridge at the output of the mixer (not represented in Fig. 2). Here, we operate at a bias voltage close to 40V for both resonators, and an excitation signal varying between 250mV and 1.2V in peak amplitude, so that we span a range of

oscillation starting below the critical Duffing amplitude and finishing above.

The duty cycle of the mixer outputs (and hence the phase-difference between the resonators), and the RMS voltages at the output of the readout are measured with an MSO5204B oscilloscope. This lets us plot the evolution of the phase-difference and amplitude-ratio output metrics versus the detuning voltage, in the linear and nonlinear operation regimes. The results are reported in section IV.

II. MODELING

Provided the mechanical oscillation amplitude is small with respect to the electrostatic gap, the actuation nonlinearity can be neglected [11]. The system can then be modeled as two Duffing resonators, nonlinearly-coupled via the digital mixing stage. Following the harmonic balance approach of [5], a set of 4 (non-dimensionalized) equations is found:

$$\left(1+\frac{3}{4}\gamma X^2-\omega^2\right)X=\frac{F}{\pi}\left(\cos\psi+\cos\left(\psi+\phi\right)\right) \tag{1}$$

$$\frac{\omega}{Q}X=\frac{F}{\pi}\left(\sin\psi+\sin\left(\psi+\phi\right)\right) \tag{2}$$

$$\left(1-\varepsilon+\frac{3}{4}\gamma Y^2-\omega^2\right)Y=\frac{F}{\pi}\left(\cos\psi-\cos\left(\psi-\phi\right)\right) \tag{3}$$

$$\frac{\omega}{Q}Y=\frac{F}{\pi}\left(\sin\psi-\sin\left(\psi-\phi\right)\right) \tag{4}$$

where the state of the system consists in mechanical oscillation amplitudes X and Y, oscillation pulsation ω and phase difference ϕ, where F is the magnitude of the excitation force, proportional to the excitation voltage, Q is the quality factor of the resonators, ε is a detuning parameter, set by the bias voltage of the second resonator, γ is the *negative* Duffing coefficient, and $\psi=\pi/4$ is the phase difference between the comparator output and the mechanical motion of the resonator. For a given set of parameters, the state must usually be solved for with numerical methods.

When $\varepsilon=0$, the nominal state of the system verifies

$$\phi=\pi/2\,,\ X/Y=1\,. \tag{5}$$

The stability of the synchronized state can be assessed by a dynamic perturbation approach, as in [5]. This boils down to verifying that the roots of the characteristic polynomial

$$P(\lambda)=\lambda^2+\lambda\times\frac{1}{2Q}\left(3-\frac{1}{\sin\phi}\right)+\frac{1}{4Q^2}\left(\frac{2}{1+\sin\phi}-\frac{3}{2}\gamma\frac{Q^3}{\omega^3}\frac{F^2}{\pi^2}\left(2\sin^2\phi+\sin\phi-1\right)\right) \tag{6}$$

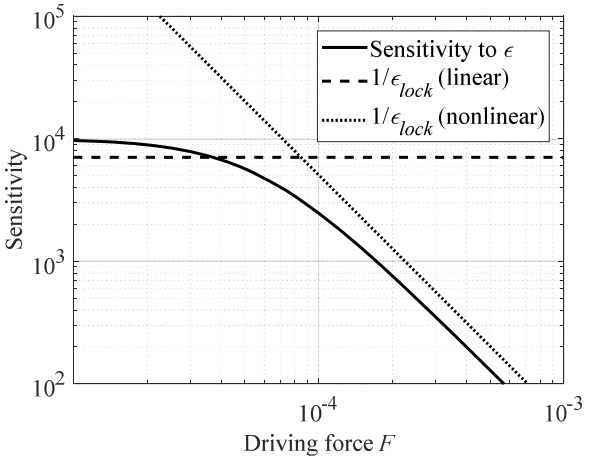

Fig. 4. Sensitivity to mismatch of the amplitude ratio and phase difference output metrics, versus driving force.

have negative real parts. From (6), it is plain that, when $\gamma=0$, the locking range (in terms of phase) is set by

$$\phi\in\left[\sin^{-1}\left(\frac{1}{3}\right),\pi-\sin^{-1}\left(\frac{1}{3}\right)\right]\approx\left[20°,160°\right]. \tag{7}$$

In the nonlinear regime, stability is governed by the sign of the term in factor of γ in (6), so that the synchronization range is then slightly reduced to:

$$\phi\in\left[\frac{\pi}{6},\frac{5\pi}{6}\right]=\left[30°,150°\right]. \tag{8}$$

Although the bounds on ϕ vary little from one regime to the other, those on ε are drastically changed. This is readily seen by subtracting (3) from (1), which yields:

$$\varepsilon=\frac{3}{4}\gamma\left(X^2-Y^2\right)+\frac{2}{Q}\frac{\cos\phi}{1+\sin\phi} \tag{9}$$

assuming $\omega\approx1$. In the linear regime, the first term on the right-hand side of (9) can be neglected, and (7) then corresponds to a measurement range

$$\left|\varepsilon\right|\le\varepsilon_{lock}=\frac{\sqrt{2}}{Q}. \tag{10}$$

whereas in the nonlinear regime, using (2) and (4) to express X and Y as functions of ϕ, (9) implies that

$$\left|\varepsilon\right|\le\varepsilon_{lock}=\frac{9\sqrt{3}}{8}\left|\gamma\right|\left(\frac{QF}{\pi}\right)^2. \tag{11}$$

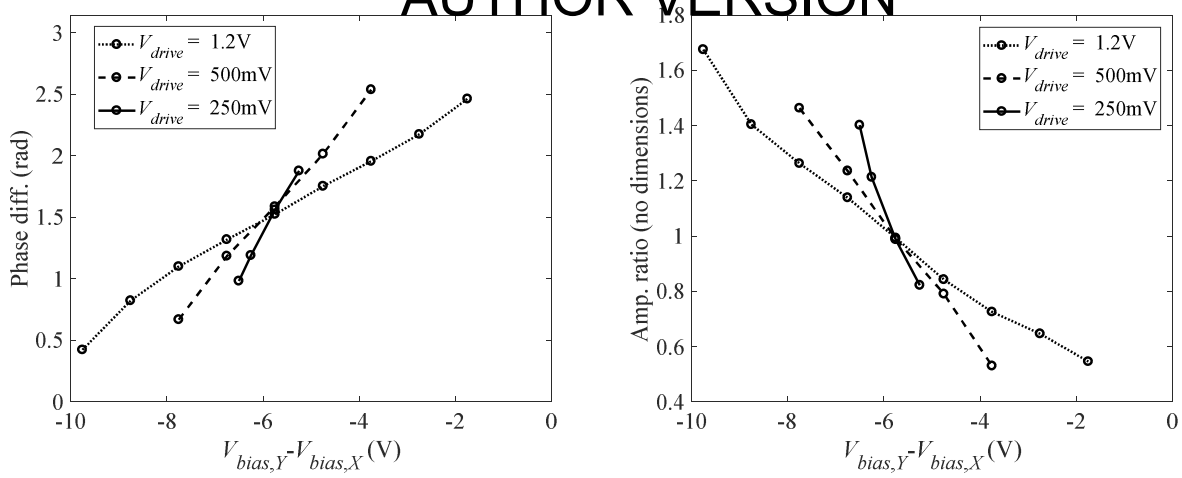

Fig. 5. Measured values of the phase difference (left) and amplitude ratio (right) output metrics vs. bias voltage difference for different values of the drive voltage.

These results, in agreement with [8-9], show that operating the MILO in the nonlinear regime is beneficial in terms of measurement range, with an obvious trade-off in terms of sensitivity to mismatch. Moreover, this is also true for the amplitude ratio output metric, which can be expressed simply as a function of ϕ by dividing (2) by (4). In particular, for the MILO considered here, the sensitivity to ε of the amplitude ratio close to $\varepsilon = 0$ is equal (in absolute value) to that of the phase difference. However, it should be noted that these output metrics have different sensitivities to additive random fluctuations, as shown in [10].

It is worth insisting that the nonlinear stability bounds established above are only valid when the Duffing coefficient γ is negative. In the case of a hardening Duffing nonlinearity, large-amplitude oscillation is not possible for the architecture considered here. This is readily seen by considering the $\varepsilon = 0$ case and letting $\phi = \pi/2$ in (6): for positive γ, the 0th-degree term of $P(\lambda)$ is cancelled out when

$$F \approx \pi / \sqrt{3\gamma Q^3} \,, \tag{12}$$

and the nominal steady-state solution (5) is unstable for larger values of the driving force. Thus, in order to operate beyond the critical Duffing amplitude, the parameters of a MILO should be chosen depending on the hardening or softening character of the nonlinearity. For example, the architecture described in section II with $\psi = \pi/4$ phase-shift in each branch is well-adapted to softening nonlinearities. But setting the phase-shift to $\psi = 3\pi/4$, so that the nominal state of the system is

$$\phi = -\pi/2 \,,\; X/Y = 1 \,, \tag{13}$$

leads to an architecture which is equally well-adapted to hardening nonlinearities.

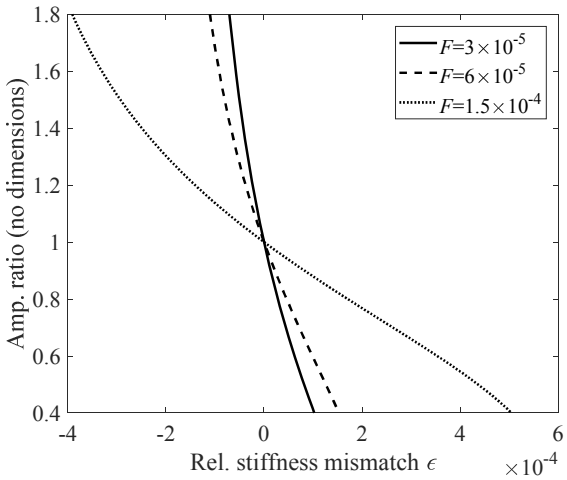

Fig. 6. Simulated value of the amplitude ratio vs. relative stiffness mismatch for different values of the driving force.

Illustrations of these theoretical results are given in the next section.

III. ILLUSTRATIONS AND RESULTS

We represent in Fig. 4 the sensitivity to ε of the phase difference and of the amplitude ratio output metrics, i.e.

$$\left.\frac{\partial\phi}{\partial\varepsilon}\right|_{\varepsilon=0} = -\left.\frac{\partial(X/Y)}{\partial\varepsilon}\right|_{\varepsilon=0} \tag{14}$$

versus the driving force F. System parameters are $Q = 10^4$, $\gamma = -10^{-3}$, which roughly corresponds to the parameters of the experimental setup at the chosen bias voltage [11]. One verifies that the sensitivity at $\varepsilon = 0$ is inversely proportional to the locking range ε_{lock} (10-11).

Similar results are obtained with the experimental setup of section II, as illustrated in Fig. 5. First of all, the bias voltage range over which the resonators remain synchronized clearly increases with the driving voltage. The nearly linear relation between the locking range and the drive amplitude indicates that the measurements correspond to a transition from the linear regime to the nonlinear regime, as Fig. 4 suggests. As a basis for comparison, the results obtained with our model and drive amplitudes $F = 3\times10^{-5}$, $F = 6\times10^{-5}$ and $F = 1.5\times10^{-4}$ are represented in Fig. 6, showing good qualitative agreement.

Discrepancies between our model and our measurements can be explained by several reasons. First of all, in this experiment, the bias voltage control was rather crude (100mV accuracy, controlled manually), which made it delicate to span the locking range, in particular when the sensitivity to mismatch is large, i.e. at small drive amplitudes. Furthermore, near the edges of the locking range, the amplitude of one of the motional signals decreases, so that the delay introduced by the comparator hysteresis becomes significant in that branch of the MILO, causing increased imbalance and reducing the locking range. This is also particularly true at smaller drive amplitudes. Finally, it should be pointed out that our idealized model assumes both resonators are identical (same quality factor, same Duffing coefficient, same actuation force) although this is not the case in the experimental setup: in particular several phenomena are neglected in the model, as the dependence of the Duffing coefficient and of the driving force on bias voltage (hence, on ε).

IV. Conclusion

We have presented in this paper a theoretical and experimental study of the properties of a MILO-based architecture, when the resonators are pushed into the nonlinear regime. It was shown that an increase of the synchronization range results from operating this architecture in the nonlinear regime.

Our experimental measurements are in good agreement with the idealized model results, showing the expected tradeoff between synchronization range and sensitivity [8-10]. Furthermore, the experimental results point out that operating at a larger amplitude makes it possible to relax the constraints of the electronic part of the system. Finally, our results confirmed that the amplitude ratio and phase difference output metrics are equivalent as far as sensitivity is concerned. However, it should be pointed out that these quantities are not equivalent as far as sensitivity to random fluctuations is concerned (e.g. thermomechanical noise), as shown in [10].

References

[1] C. Zhao et al., "A review on coupled MEMS resonators for sensing applications utilizing mode localization," Sensors and Actuators A: Physical, vol. 249, pp. 93-111, 2016.

[2] P. Thiruvenkatanathan, J. Yan and A. A. Seshia, "Differential amplification of structural perturbations in weakly coupled MEMS resonators," IEEE Transactions on Ultrasonics, Ferroelectrics 9and Frequency Control, vol. 57, pp. 690-697, 2010.

[3] C. Zhao et al., "A closed-loop readout configuration for mode-localized resonant MEMS sensors" IEEE Journal of Microelectromechanical Systems, vol. 26, pp. 501-503, 2017.

[4] C. Zhao et al. "Experimental Observation of Noise Reduction in Weakly Coupled Nonlinear MEMS Resonators", IEEE Journal of Microelectromechanical Systems, vol. 26, pp. 1196-1203, 2017.

[5] J. Juillard, P. Prache and N. Barniol, "Analysis of mutually injection-locked oscillators for differential resonant sensing," IEEE Transactions on Circuits and Systems I: Regular Papers, vol. 63, pp. 1055-1066, 2016.

[6] P. Prache, et al., "Design and characterization of a monolithic CMOS-MEMS mutually injection-locked oscillator for differential resonant sensing", Sensors and Actuators A: Physical, vol. 269, pp. 160-170, 2017.

[7] J. Juillard, P. Prache, P.M. Ferreira, N. Barniol, "Ultimate limits of differential resonant MEMS sensors based on two coupled resonators", IEEE Transactions on Ultrasonics, Ferroelectrics and Frequency Control, 2018 (accepted).

[8] O. Shoshani, et al. "Phase noise reduction in a MEMS oscillator using a nonlinearly enhanced synchronization domain", IEEE Journal of Microelectromechanical Systems, vol. 25, pp. 870-876, 2016.

[9] P Taheri-Tehrani, M Defoort, DA Horsley, "Synchronization of a micromechanical oscillator in different regimes of electromechanical nonlinearity", Applied Physics Letters, vol. 111, pp. 183503, 2017.

[10] J. Juillard, A. Mostafa, P. M. Ferreira, "Analysis of resonant sensors based on mutually injection locked oscillators beyond the critical Duffing amplitude", European Frequency and Time Forum, 2018 (accepted).

[11] A. Brenes, J. Juillard, L. Bourgois, F. Vinci dos Santos, "Influence of the driving waveform on the open-loop frequency response of MEMS resonators with nonlinear actuation schemes", IEEE Journal of Microelectromechanical Systems, vol. 25, pp. 812-820, 2016.